

Prospects for Detecting Neutrino Signals from Annihilating/Decaying Dark Matter to Account for the PAMELA and ATIC results

Jia Liu, Peng-fei Yin and Shou-hua Zhu

*Institute of Theoretical Physics & State Key Laboratory of Nuclear Physics and Technology,
Peking University, Beijing 100871, P.R. China*

(Dated: February 12, 2022)

Recent PAMELA data show that positron fraction has an excess above several GeV while anti-proton one is not. Moreover ATIC data indicates that electron/positron flux have a bump from 300 GeV to 800 GeV. Both annihilating dark matter (DM) with large boost factor and decaying DM with the life around $10^{26}s$ can account for the PAMELA and ATIC observations if their main final products are charged leptons (e , μ and τ). In this work, we calculated the neutrino flux arising from μ and τ which originate from annihilating/decaying DM, and estimated the final muon rate in the neutrino telescopes, namely Antares and IceCube. Given the excellent angular resolution, Antares and IceCube are promising to discover the neutrino signals from Galactic center and/or large DM subhalo in annihilating DM scenario, but very challenging in decaying DM scenario.

PACS numbers: 95.35.+d, 13.15.+g, 95.55.Vj, 98.62.Gq

I. INTRODUCTION

The main components of our Universe are ‘dark’. Many astrophysical observations have confirmed the existence of dark matter (DM) which contributes roughly 23% to the energy density of the Universe. If the DM are weakly interacting massive particles (WIMPs), they would annihilate into gamma rays, neutrinos and anti-matter particles, which could be detected experimentally. Generally speaking, the DM should be stable compared with the life of the Universe. However it is possible that the DM is decaying at an extremely low rate. Similarly, the DM decay products can be observable.

Recently PAMELA released their first cosmic rays results on the positron and anti-proton ratios [1]. Usually the anti-matter particles are expected to be produced when the cosmic rays propagate in the Galaxy and interact with the interstellar medium. The PAMELA data show a clear upturn (excess) on the positron ratio above ~ 10 GeV up to ~ 100 GeV. Besides PAMELA observation, ATIC collaboration also reported an electron/positron excess around $300 \sim 800$ GeV [2]. Contrary to the excess of position ratio, PAMEMA anti-proton ratio is consistent with the predictions. Both PAMELA and ATIC observations indicate some unknown high energy primary positron sources in the Galaxy. Studies showed that the pulsars or other nearby astrophysical sources may account for the PAMELA results [3].

Other possibility to induce the positron excess can be the annihilating [4, 5, 6] or decaying [7] DM in the Galaxy. In the annihilating DM scenario, if the cross section $\langle\sigma v\rangle$ is taken as the typical annihilation cross section $\sim 3 \times 10^{-26} cm^3 s^{-1}$ for thermal relic, a large extra boost factor (BF) is needed to produce sufficient positron flux to fit the PAMELA results. Many ideas are proposed to induce the large BF. For example, the new ‘long’ range force would enhance the annihilation cross section for today low velocity DM, which is dubbed as ‘Sommerfeld effect’ [5, 6, 8, 9]. For the decaying DM scenario, by adjusting the lifetime of the DM, no BF is needed. Contrary to positron excess, no obvious anti-proton excess has been observed. This suggests that the main final products from the annihilation or decay of DM are charge leptons (e , μ and τ) for $m_{DM} < 1TeV$. Otherwise one needs much heavy DM, say $O(10TeV)$ [5], or some special cosmic-ray propagation parameters.

Provided that charged leptons are generated by DM annihilating and/or decaying DM, it is quite interesting to investigate which charged leptons are response for the PAMELA and ATIC observations. It is natural to expect that the high energy charged leptons are

correlated to other observable signals, such as gamma rays, synchrotron emissions or neutrinos. Detecting neutrino signals from DM is very attractive and useful to pin down the nature of DM. In this paper, we will calculate the neutrino flux from the μ and τ which are producing by DM. Unlike other DM related products, neutrinos have less trajectory deflection and less but finite energy loss [10] during propagation, due to their weakly interaction nature. As a result, the neutrinos can keep the important information of the DM. For the same reason, the neutrinos are difficult to be detected if the flux is low (for some recent works, see [11, 12, 13, 14, 15, 16]). Usually the neutrinos detected by neutrino telescopes, such as Super-Kamiokande [17, 18], AMANDA [19] etc. are expected to be the atmospheric neutrinos, which are produced by interaction between the cosmic rays and atmosphere. The atmospheric neutrinos are the main backgrounds for detecting the extra neutrinos from DM. Currently, no high energy astrophysical neutrinos have ever been detected [20].

If the charged leptons are indeed produced by DM, it is a good news for neutrino detection. Firstly, the neutrino flux can be much larger than that of usual expected. The PAMELA and ATIC data need higher primary positron production rate than usual production, thus it is natural to expect that large neutrino flux can be produced from μ and τ decays. Secondly, the heavy DM (e.g. $\sim TeV$) is favored by ATIC result, thus the neutrinos at the similar energy scale are expected. As the main backgrounds, the atmospheric neutrino flux decreases logarithmically with the increment of energy, thus higher energy neutrinos correspond to less backgrounds. On-going and future kilometer size neutrino telescopes such as Antares [21], IceCube [22] and KM3NeT [23] can better explore these signals. Thirdly, in the annihilating DM scenario, the flux of neutrinos depends on the square of the DM number density. If one searches the Galactic center (GC) or large DM subhalos which contain the denser DM than other areas, large neutrino flux can be produced. Moreover if the Sommerfeld effect of DM annihilation is true, the DM annihilation in the subhalo can acquire even larger BF due to the lower velocity dispersion than that in the DM halo [6, 9]. As a side remark, this feature provides a potential method to distinguish two DM scenarios, namely GC or DM subhalos can be higher flux neutrino sources in the annihilating DM scenario than those in the decaying DM one.

This paper is organized as following. In section II, we calculated the neutrino flux from the GC and DM subhalo, in the model-independent manner, in the annihilating and decaying DM scenarios. In section III, we estimated the muon rate at Antares and IceCube for the

two DM scenarios. We pointed out that Antares and IceCube might detect neutrino signals in annihilating DM scenario and distinguish different DM scenarios. Section IV contains our discussions and conclusions.

II. NEUTRINO SIGNALS FROM ANNIHILATING/DECAYING DM

PAMELA data show an excess on positron fraction about $10 \sim 1000$ times larger than usual estimation, so it is natural to expect that the neutrinos from DM are also enhanced by the similar number. In the annihilating DM scenario, it is achieved by Sommerfeld enhancement and/or clumps in DM density. In this paper, BF is used to denote the Sommerfeld enhancement. Astrophysical enhancement is contained in the astrophysical factor, as described below.

The neutrino flux observed on the Earth can be written as

$$\phi^A(E, \theta) = \rho_\odot^2 R_\odot \times \frac{1}{4\pi} \frac{\langle \sigma v \rangle}{2m_\chi^2} \frac{dN}{dE} \times J^A(\theta) \quad (1)$$

and

$$\phi^D(E, \theta) = \rho_\odot R_\odot \times \frac{1}{4\pi} \frac{1}{m_\chi \tau_\chi} \frac{dN}{dE} \times J^D(\theta), \quad (2)$$

with dimensionless $J^A(\theta)$ and $J^D(\theta)$ defined as

$$J^A(\theta) = \frac{1}{\rho_\odot^2 R_\odot} \int_{LOS} \rho^2(l) dl \quad (3)$$

$$J^D(\theta) = \frac{1}{\rho_\odot R_\odot} \int_{LOS} \rho(l) dl. \quad (4)$$

Here 'A' and 'D' denote annihilating and decaying DM respectively. $\rho_\odot = 0.34 \text{ GeV cm}^{-3}$ is the local DM density and $R_\odot = 8.5 \text{ kpc}$ is the distance between the Sun and the GC. θ is defined as the angle between the observational and the GC directions, m_χ is the mass of DM particle, and dN/dE is the energy spectrum of ν per annihilation or decay. $\langle \sigma v \rangle$ is the thermally averaged annihilation cross section, which can be written as

$$\langle \sigma v \rangle = \langle \sigma v \rangle_0 \times BF. \quad (5)$$

Here $\langle \sigma v \rangle_0$ is set to be $3 \times 10^{-26} \text{ cm}^3 \text{ s}^{-1}$, which is the typical annihilation cross section for the present dark matter abundance under the standard thermal relic scenario. Thus the number BF is enhancement factor compared with the typical value. The BF can arise from the

Sommerfeld enhancement as described above. The integral path in Eqs. (3) and (4) is along the line-of-sight (LOS). The neutrino spectrum dN/dE comes from μ, τ decay. We count all three flavor of neutrinos and anti-neutrinos at the decay point. After vacuum oscillation, we adopt assumption that the three flavor neutrinos have the equal flux [11]. Thus we multiply a factor of 1/3 in order to get the flux of muon neutrino and anti-muon neutrino, which is the main measured component in the neutrino detector. We should mention here that the tau neutrinos can also be observed by the Cherenkov neutrino detector because tau neutrino has the different signal compared with muon neutrino. The tau neutrino can interact with nucleons and produce tau leptons which subsequently decay into muons. Thus they will produce a kink in the reconstruction by Cherenkov light, while the muon neutrino has no such kink. The authors of Ref. [16] have discussed the tau neutrino from decaying dark matter and found it can improve the detection by a few orders of magnitude. The reason is simply that the atmospheric neutrinos has much less tau neutrinos than muon neutrinos at high energy. In this paper, we will concentrate on muon neutrinos observation.

The solid angle average of this J factor is defined as

$$J_{\Delta\Omega}^{A,D} = \frac{1}{\Delta\Omega} \int_{\Delta\Omega} J^{A,D}(\theta) d\Omega \quad (6)$$

with $\Delta\Omega = 2\pi(1 - \cos\theta)$. The averaged neutrino flux in a certain cone can be written as

$$\phi_{\Delta\Omega}^A(E) = \rho_{\odot}^2 R_{\odot} \times \frac{1}{4\pi} \frac{\langle\sigma v\rangle}{2m_{\chi}^2} \frac{dN}{dE} \times J_{\Delta\Omega}^A \quad (7)$$

$$\phi_{\Delta\Omega}^D(E) = \rho_{\odot} R_{\odot} \times \frac{1}{4\pi} \frac{1}{m_{\chi}\tau_{\chi}} \frac{dN}{dE} \times J_{\Delta\Omega}^D. \quad (8)$$

In order to calculate the neutrino flux, we must know both the astrophysical $J_{\Delta\Omega}$ factor and the neutrino spectrum from charged leptons. In Fig. 1, we plot the $J_{\Delta\Omega}$ factor for annihilating and decaying DM respectively. We used NFW [24] profile here. From the figure we can see that the $J_{\Delta\Omega}$ reach its maximum values, around 1000 and 20 for annihilating and decaying DM, in the direction of GC as expected. If cusped density like Moore profile is used, one will get much larger and slightly larger $J_{\Delta\Omega}$ factors for annihilating and decaying DM respectively. However, some authors [25] suggested that DM halos around galaxies have the shallower density than that of predicted by standard cold dark matter theory.

Besides the GC, subhalos can also be the high energy neutrino sources. In the direction of the DM subhalos, $J_{\Delta\Omega}$ factor can be easily as large as 100, or even higher. In order to

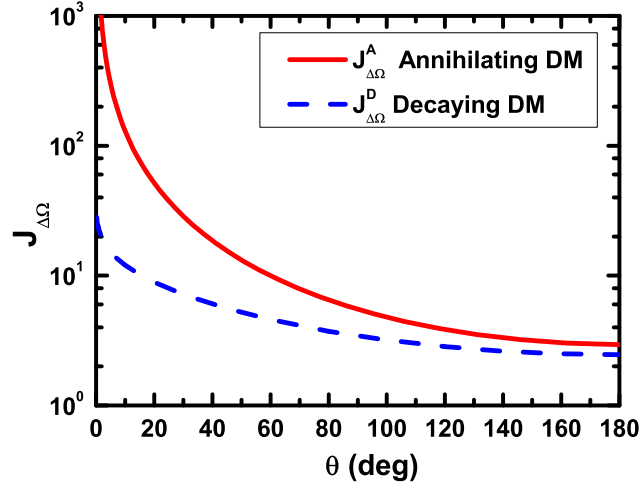


FIG. 1: $J_{\Delta\Omega}$ for annihilating and decaying DM as the function of half-angle θ for the cone centered at the direction of the GC. The DM distribution adopted here is NFW profile.

keep the line of this paper, we put the analysis on the number distribution of large $J_{\Delta\Omega}$ subhalo in the Galaxy in the Appendix.

In Fig. 2, the positron fraction from pure muon and tau decays, as well as the energy spectrum of positron/electron are plotted for annihilating and decaying DM. It is a model-independent discussion of these charged lepton channels, thus we assumed that $\chi\chi \rightarrow l\bar{l}$ for annihilating DM and $\chi \rightarrow l\bar{l}$ for decaying DM respectively. From the figures, we can see that these channels can account for both the PAMELA and ATIC data with the proper parameters. In the following calculation of neutrino flux, we use the same set of parameters to get the neutrino spectrum dN/dE .

Based on the $J_{\Delta\Omega}$ factor and the neutrino spectrum from charged leptons, we can calculate the neutrino flux. In Fig. 3, the expected neutrino flux from muon and tau decay for annihilating and decaying DM from the GC are plotted. We choose the half angle θ to be 10° which is the angular resolution of Super-K for the neutrino energy from 1 GeV to 10 GeV for a conservative analysis [18]. For the neutrino with higher energy, the Super-K is difficult to measure the energy of the muons but can count the number. The parameters BF and life of DM are taken to be the values which can account for the PAMELA and ATIC data. The figures show that the two DM scenarios have comparable average neutrino flux with that of the atmospheric neutrino [26] for high energy neutrino, because of the logarithmic decrease

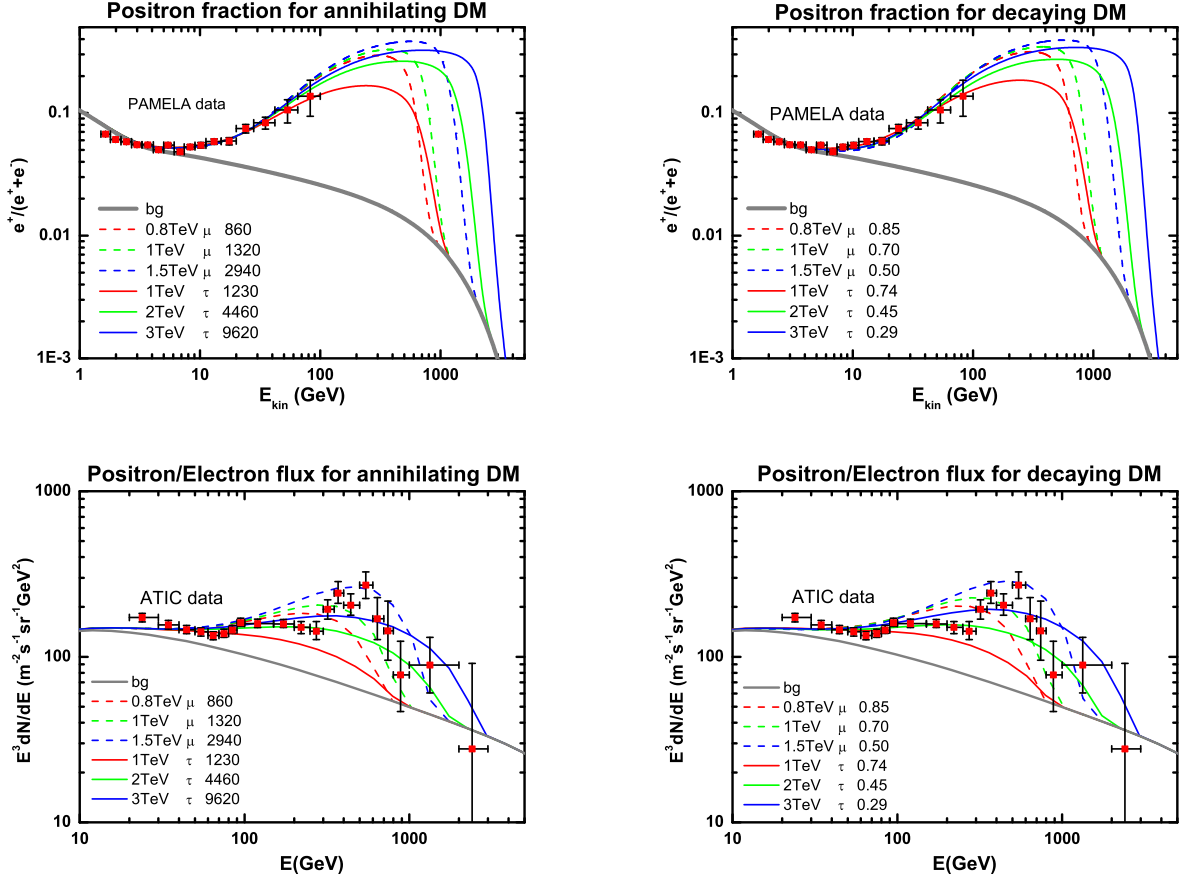


FIG. 2: The positron fraction from pure muon and tau decays, as well as the positron/electron energy spectrum for annihilating and decaying DM to account for PAMELA and ATIC data. In the figures, the labels on the left, e.g. 0.8 TeV, are the energy of the muon or tau leptons, while the labels on the right, e.g. 860 or 0.85, are the boost factor or life in unit of $10^{26}s$ for annihilating DM and decaying DM respectively.

of the atmospheric neutrino. For the low energy region, the neutrino flux are much smaller than that of the atmospheric neutrino. For some heavy DM, the Super-K can even place the constraints [11, 14] on their annihilating cross section or life [13]. For the smaller cone with $\theta = 2^\circ$, high energy neutrino from the annihilating DM have much larger flux than that from the background.

In the subhalo, the Sommerfeld enhancement for the DM annihilation can be larger than that in the halo because the relative velocity of the DM particles are lower. For example the subhalos can have the velocity dispersion of $O(10)km/s$ [28], which is smaller than the

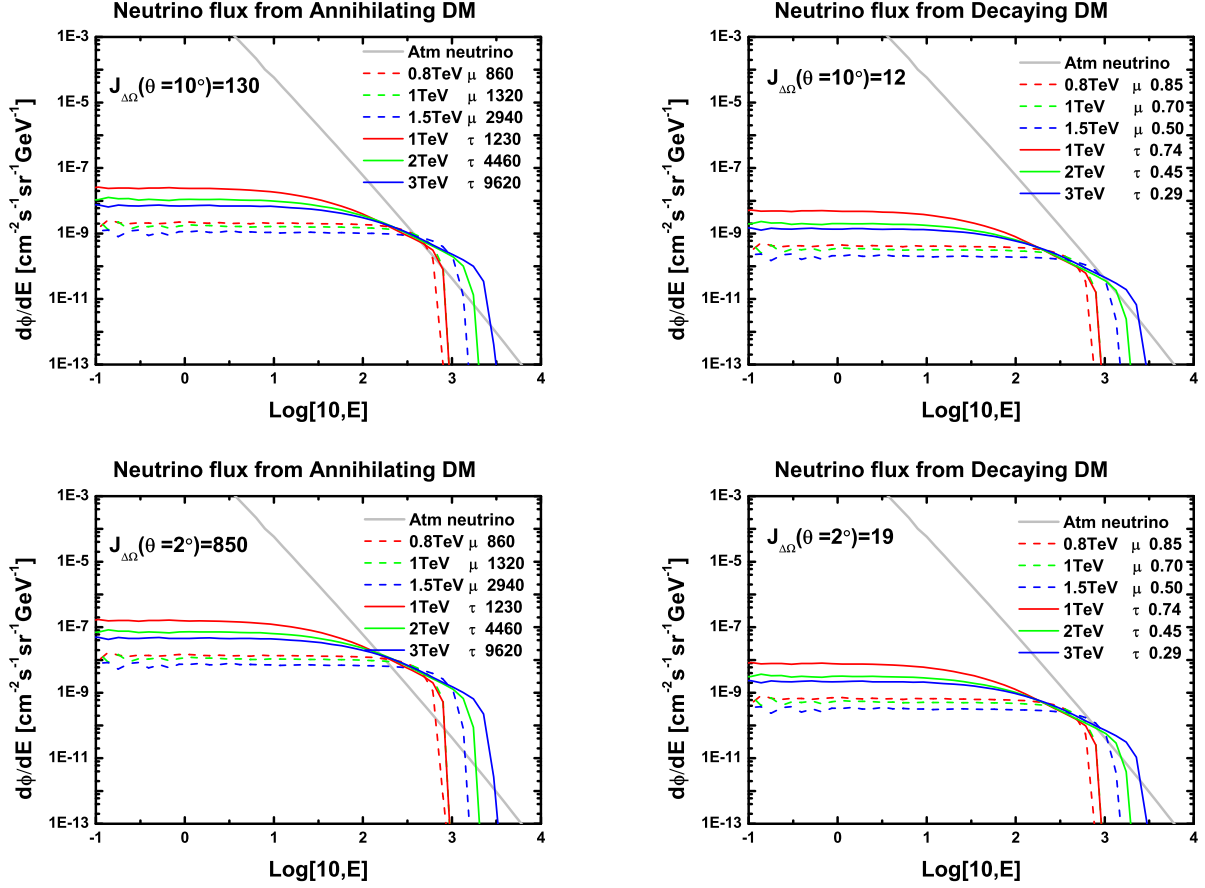


FIG. 3: The muon and anti-muon neutrino flux for annihilating and decaying DM at the GC. The atmospheric neutrino flux data is from Ref. [26]. The x-axis is the energy of neutrinos and the half angle θ is 10° and 2° respectively. Other labels in the figure are similar with Fig. 2.

usual velocity of DM $v \sim 10^{-3}c \sim 300km/s$. Thus one can expect an extra Sommerfeld enhancement for the subhalo [6, 9]. The larger BF in the subhalo will not contradict with the current atmospheric data, since this effect will be diluted with the larger cone angle where J factor decreases rapidly. In this paper we do not adopt this extra enhancement, however we note here that such enhancement can make the discovery of neutrino from subhalo in annihilating DM scenario even more promising. The decaying DM have much smaller J factor for massive subhalo, since it does not benefit from the cusped profile very much. Thus it is possible to detect neutrino from subhalo in annihilating DM scenario, but very challenging in decaying DM scenario.

III. MUON RATE AT NEUTRINO TELESCOPES

The neutrino detector Antares have angular resolution of 2° from 100GeV to 1TeV [27] and can see GC for 63% of a year [21]. The Antares has about eight years of operation time from 2007 to 2015. Using the neutrino effective area $A_v^{eff}(E)$ of Antares [29], we calculate the events in the 2° cone in the Table. I for annihilating DM. The total number of events is $N_v = \int A_v^{eff}(E) \frac{d\phi_v}{dE} dE$. From the table, we can see that Antares may discover the neutrino signal from GC in annihilating DM scenario, but difficult in decaying DM scenario because the signal gets negligible increase from smaller cone, which can be seen in the lower panel of Fig. 3. The future neutrino detector like KM3NeT can further explore the annihilating DM scenario.

channel	N	σ	channel	N	σ
atm	1.5	—	atm	1.5	—
0.8TeV μ	7.7	6.2	1TeV τ	12.2	9.9
1TeV μ	16.5	13.4	2TeV τ	21.2	17.2
1.5TeV μ	29.4	23.9	3TeV τ	23.3	18.9

TABLE I: The neutrino event numbers in the energy interval $500GeV - 1TeV$ for eight years of Antares operation from the 2° cone in the GC direction. σ is the significance defined as S/\sqrt{B} .

IceCube locates in the south pole and covers the northern sky. It is excellent to look at the possible large DM subhalo in the Galaxy, provided that it has good angular resolution like 1° [22], which can greatly suppress the atmospheric neutrino background. The massive DM subhalo can have high density in the center, thus it can produce large neutrino flux and can be identified by the high resolution neutrino detector like IceCube. Subhalo can easily reach large J factor, say $J_{\Delta\Omega}^{Subhalo}(\theta = 1^\circ) \sim 100$ or even larger values [15]. In the Appendix, the number distribution of massive DM subhalos in our Galaxy has been discussed in detail. In the following estimation, we do not adopt the extreme subhalo model, instead we take J factor equal to 100.

For the IceCube, we use the same method in Ref. [12, 14] to estimate the muon rate in the neutrino telescopes in annihilating DM scenario. The total muon and anti-muon rate is

expressed as following,

$$\frac{dN_\mu}{dE_\mu} = \int_{E_\mu}^{\infty} \frac{d\phi_{\nu_\mu}}{dE_{\nu_\mu}} \left[\frac{d\sigma_\nu^p(E_{\nu_\mu}, E_\mu)}{dE_\mu} \rho_p + \frac{d\sigma_\nu^n(E_{\nu_\mu}, E_\mu)}{dE_\mu} \rho_n \right] R_\mu(E_\mu) A_{eff}(E_\mu) dE_{\nu_\mu} + (\nu \rightarrow \bar{\nu}), \quad (9)$$

where $d\phi_{\nu_\mu}/dE_{\nu_\mu}$ is the muon neutrino flux arrived at the neutrino detector. $d\sigma_\nu^p(E_{\nu_\mu}, E_\mu)/dE_\mu$ and $d\sigma_\nu^n(E_{\nu_\mu}, E_\mu)/dE_\mu$ are differential cross sections for the muon production process $\nu p \rightarrow lX$ and $\nu n \rightarrow lX$. The densities of protons and neutrons near the detector are taken to be $\rho_p = \frac{5}{9}N_A cm^{-3}$ and $\rho_n = \frac{4}{9}N_A cm^{-3}$ respectively for IceCube where detector volume is filled with ice. N_A is the Avagadro's number. The muon energy loss is given as $\frac{dE}{dx} = -\alpha - \beta E$, where α and β are empirical parameters. The distance that a muon travels in the Earth before its energy drops below threshold energy E^{thr} , is called muon range which is given as

$$R_\mu(E) = \frac{1}{\rho\beta} \ln\left(\frac{\alpha + \beta E}{\alpha + \beta E^{thr}}\right), \quad (10)$$

where we take the parameters $\alpha = 2.0 \times 10^{-6} TeV cm^2/g$ and $\beta = 4.2 \times 10^{-6} cm^2/g$ to be the same as Ref. [11]. The effective area of neutrino telescope A_{eff} is the function of muon energy which increases as the energy goes up. The symbol $(\nu \rightarrow \bar{\nu})$ means that we also count the anti-muons from the anti-muon neutrinos because the Cherenkov neutrino telescope detects both muons and anti-muons.

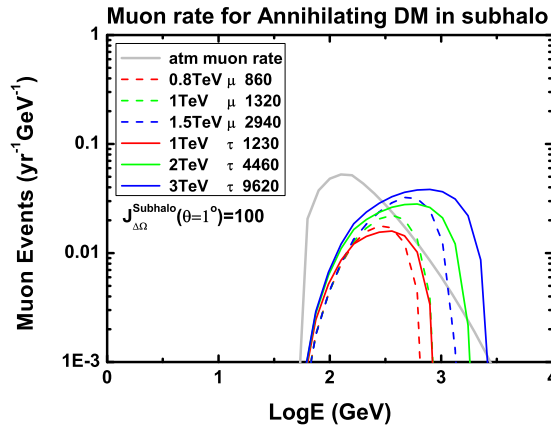


FIG. 4: The total muon and anti-muon rates for annihilating DM in the massive subhalo for the IceCube. The half angle θ is taken to be 1° .

In Fig. 4, we show the muon rate as a function of muon energy for several parameters which can account for PAMELA and ATIC data. From the figures we can see that the

signal from annihilating DM can be larger than the atmospheric background for heavy DM, even without the extra enhancement from lower velocity dispersion. We calculate the muon number in the energy interval $500\text{GeV} \sim 1\text{TeV}$ for ten years and give the significance of signal $\sigma = S/\sqrt{B}$ in the Tab. II. Heavy DM can reach the five sigma significance which is quite encouraging for subhalo neutrino search in the annihilating DM scenario. On the other hand, if no neutrino hot spots are identified, it can put constraints on subhalo model and BF for annihilating DM.

channel	N	σ	channel	N	σ
atm	57.6	—	atm	57.6	—
0.8TeV μ	21.7	2.9	1TeV τ	41.5	5.5
1TeV μ	55.2	7.3	2TeV τ	136.4	20.0
1.5TeV μ	144.9	19.1	3TeV τ	188.6	24.8

TABLE II: The total muon and anti-muon numbers in the energy interval $500\text{GeV} - 1\text{TeV}$ for ten years operation of IceCube for massive subhalo. σ is the significance defined as S/\sqrt{B} .

Finally we would like to discuss the limits from the Super-K observation. Super-K have searched neutrino signals from DM annihilation in the direction of the Sun, the Earth and the GC. Currently, no high energy astrophysical neutrinos have ever been detected. Super-K collaboration detected the upward going muons from several GeV to 10TeV in the direction of the center with half angles from 5 to 30 degrees, and set limit on muon flux [17]. For example, Super-K collaboration placed an upper bound of muon flux in the half angle 10° around the direction to the GC as $\sim 5 \times 10^{-15}\text{cm}^{-2}\text{s}^{-1}$. In our numerical examples for annihilating DM, the muon flux are $4.2 \times 10^{-15}\text{cm}^{-2}\text{s}^{-1}$, $6.5 \times 10^{-15}\text{cm}^{-2}\text{s}^{-1}$, $1.4 \times 10^{-14}\text{cm}^{-2}\text{s}^{-1}$, $5.1 \times 10^{-15}\text{cm}^{-2}\text{s}^{-1}$, $1.7 \times 10^{-14}\text{cm}^{-2}\text{s}^{-1}$ and $3.4 \times 10^{-14}\text{cm}^{-2}\text{s}^{-1}$ for 0.8TeV μ , 1TeV μ , 1.5TeV μ , 1TeV τ , 2TeV τ and 3TeV τ respectively. We should emphasize that in our calculations we have assumed that DM annihilate into pure muons or taus. If DM can annihilate to electron/positrons, it is easy to fit PAMELA and ATIC data with much smaller BF for muon and tau channels and avoid the violation of Super-K limits. On the other hand, the DM density distribution is still not very clear, especially in the central region of Galaxy and subhalos. Different DM profiles give very different contributions to $J_{\Delta\Omega}(\theta)$, especially when θ is small. For a cusped profile, the $J_{\Delta\Omega}(\theta)$ for small θ will be larger

and can compensate the decrease of BF, which can keep the neutrino signal large enough and avoid the violation of Super-K limits simultaneously. We would like to mention that more stringent constraints on the DM profile may come from the detections of gamma ray and synchrotron radiation in the GC [30].

IV. CONCLUSIONS AND DISCUSSIONS

Based on the PAMELA and ATIC observations, there may exist extra sources of charged leptons, namely electron, muon and tau. In this paper, we calculated the neutrino flux from muon and tau which arise from the annihilating/decaying DM. The final muon rate at neutrino telescopes Antares and IceCube are also estimated. Our results show that Antares is promising in discovering the neutrino signal from GC in annihilating DM scenario, but challenging in decaying DM scenario. Moreover, massive DM subhalo is also the promising high energy neutrino source in the annihilating DM scenario. For ten years operation, IceCube can reach five sigma significant neutrino signal from subhalos for heavy DM. Note that in the subhalo the extra Sommerfeld enhancement from lower velocity dispersion can further improve the neutrino signal.

In this paper we focus on the muon neutrino detection. Actually the tau neutrino is deserved further investigation because the atmospheric neutrino contains less tau neutrino than muon neutrino. If one only counts the tau numbers in the neutrino detector, it can further suppress the atmospheric background [16] and this can be done in future kilometer neutrino detector like KM3NeT. Finally, it is worthy to mention that pulsars are difficult to be detected by upcoming neutrino detector [31], thus one may distinguish it from the DM scenarios.

Acknowledgments

J. Liu and P. F. Yin thank N. Weiner for useful discussions and encouragement. We thank X. J. Bi for useful discussions. This work was supported in part by the Natural Sciences Foundation of China (No. 10775001 and 10635030).

Note added: During the completion of this work one similar analysis appeared [32]. As a cross check, we have calculated the muon flux in the 10 degree half-angle cone from the GC

for various channels, which agree with their results.

APPENDIX A: MASSIVE SUBHALO WITH LARGE $J_{\Delta\Omega}$

In order to determine the subhalo DM contributions to neutrino flux, generally speaking, we need to know the DM profile in the subhalo and the number density of subhalos in the Galaxy. Currently N-body simulations provide useful information about the DM distribution in the Galaxy. In this Appendix, we utilize the models based on N-body simulations to investigate the number distribution of the massive DM subhalo with large $J_{\Delta\Omega}$, which is defined in Eqs. (3) and (6).

1. DM subhalo profile

Based on N-body simulations, the DM distribution can usually be parameterized as,

$$\rho(r) = \frac{\rho_s}{(r/r_s)^\gamma [1 + (r/r_s)^\alpha]^{(\beta-\gamma)/\alpha}}, \quad (\text{A1})$$

where ρ_s and r_s are the scale density and scale radius parameters respectively. The parameters (α, β, γ) are $(1, 3, 1)$ and $(1.5, 3, 1.5)$ for NFW [24] and Moore [33] profiles respectively.

The two free parameters ρ_s and r_s for a subhalo can be determined once we know the subhalo mass M_v and the concentration parameter c_v which depends on the specific subhalo model. The density scale ρ_s can be determined by using the mass relation

$$\int \rho_s(r) dV = M_v. \quad (\text{A2})$$

In the following we will concentrate on how to determine r_s .

If M_v is known, we can calculate the virial radius r_v of the subhalo which is often approximated as the radius within which the average density is greater, by a specific factor $\Delta = 200$, than the critical density of the Universe $\rho_c = 139 \text{ M}_\odot \text{ kpc}^{-3}$ (M_\odot is mass of the Sun). Thus r_v can be expressed as

$$r_v = \left(\frac{M_v}{(4\pi/3)\Delta\rho_c} \right)^{1/3}. \quad (\text{A3})$$

r_v describes the radius within which the subhalo can hold together by its own gravity, but it does not describe how the DM mass are distributed inside the distance r_v . On the other

hand, the scale radius r_s describes the DM mass distribution in the subhalo that most of mass are within this radius. The concentration models assume that the r_s is proportional to the r_v and determine ratio of them. Large ratio of r_v/r_s represents the mass of subhalo are highly concentrated in a small radius in the center, which results in the cusped profile.

For a concentration model the ratio of r_v/r_s is closed related to concentration parameter c_v , which is defined as $c_v = \frac{r_v}{r_{-2}}$. Here r_{-2} is another radius parameter which is defined as $\frac{d}{dr}(r^2\rho)|_{r=r_{-2}} = 0$. r_{-2} represents the radius within which the mass of the subhalo is concentrated. To illustrate this point, we can easily check that r_{-2} is in fact the inflexion point of the mass, i.e. $\frac{d^2M(r)}{dr^2}\Big|_{r=r_{-2}} = 0$ with $M(r) = \int_0^r \rho(r') \cdot 4\pi r'^2 dr'$. The relation between r_{-2} and r_s can be calculated by the definition of r_{-2} and Eq. (A1). The r_s for NFW and Moore profiles are $r_s^{nfw} = r_{-2}$ and $r_s^{moore} = r_{-2}/0.63$ respectively. Thus the r_s can be determined by M_v , i.e.

$$r_s^{nfw} = \frac{r_v(M_v)}{c_v(M_v)}, \quad r_s^{moore} = \frac{r_v(M_v)}{0.63 c_v(M_v)}. \quad (\text{A4})$$

Based on the above description, we can see that once the $c_v - M_v$ relation is given by the concentration model, the DM profile of subhalo is determined.

We use the same method as Ref. [15] which adopts two concentration models, which are ENS01 [34] and B01 [35]. In the Ref. [36], the c_v is fitted in a polynomial form as

$$\ln(c_v) = \sum_{i=0}^4 C_i \times \left[\ln \frac{M_v}{M_\odot} \right]^i, \quad (\text{A5})$$

where $C_i = \{3.14, -0.018, -4.06 \times 10^{-4}, 0, 0\}$ and $\{4.34, -0.0384, -3.91 \times 10^{-4}, -2.2 \times 10^{-6}, -5.5 \times 10^{-7}\}$ for ENS01 and B01 model respectively.

In Fig. 5, the scale radius r_s as a function of subhalo mass M_v is plotted to show how large the subhalos are. The subhalo radius is smaller in B01 model than that in ENS01 model because the c_v is larger in B01 model. This plot assumes that subhalos have NFW profile. For the Moore profile r_s^{moore} is equal to $r_s^{nfw}/0.63$.

2. Subhalo number distribution

The number of subhalos has been revealed by many N-body simulations [37]. The number density of subhalos have a power-law relation with subhalo mass and an uniform distribution

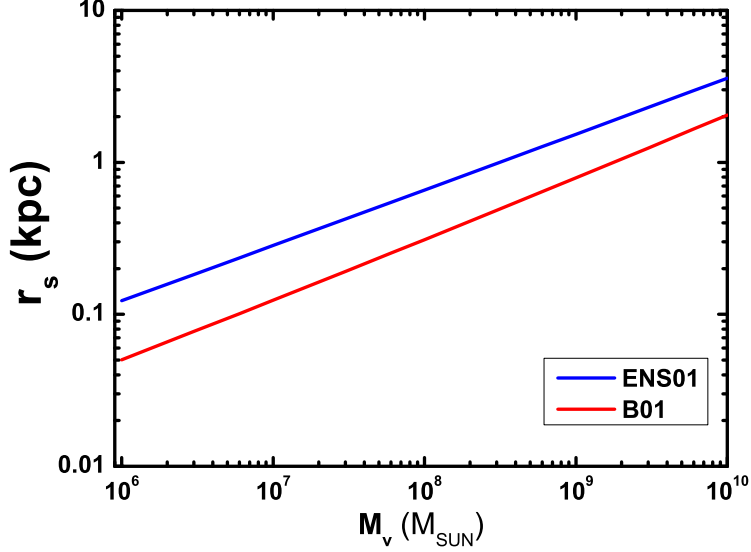


FIG. 5: The scale radius r_s as a function of subhalo mass M_v .

in the solid angle as,

$$\frac{dN}{dM_v \cdot 4\pi r^2 dr} = N_0 \left(\frac{M_v}{M_{host}} \right)^{-\alpha} \frac{1}{1 + \left(\frac{r}{r_H} \right)^2}, \quad (\text{A6})$$

where r is the distance from the GC to subhalo, M_{host} is the mass of host halo (the virial mass of the Galaxy of $M_{host} = 10^{12} M_\odot$). r_H is the core radius which is usually a fraction of the virial radius of the host halo (The relation $r_H \approx 0.14 r_v$ is adopted here [38]). The slope α varies from 1.7 to 2.1, and an intermediate α is adopted, i.e. $\alpha = 1.9$ [39]. N_0 is the normalization factor which is determined by setting the number of subhalos with mass larger than $10^8 M_\odot$ to be 100 [36]. Thus if M_v and the distance r of the subhalo are known, we can calculate the number density of the subhalos.

3. Number of subhalos with $J_{\Delta\Omega(1^\circ)} > 100$

In this subsection, we will discuss the number of massive subhalo with $J_{\Delta\Omega(1^\circ)} > 100$ in our Galaxy. From the above discussions, once the concentration model (equivalently saying, the function $c_v(M_v)$) is given, the $J_{\Delta\Omega}$ is determined by M_v and the subhalo position in the

Galaxy. Generally speaking, the heavier subhalo will have larger $J_{\Delta\Omega}$. At the same time, the distance between the Earth and the subhalo is closer, the $J_{\Delta\Omega}$ will be larger.

A monte carlo method is adopted to calculate the number distribution of DM subhalos with mass larger than $10^6 M_\odot$, according to the distribution function Eq. (A6). Besides M_v and subhalo distance r from GC, we still need the azimuthal angles θ and ϕ , which are uniformly distributed in the solid angle to specify the position of the subhalo. Once we know the above four parameters, the $J_{\Delta\Omega}$ can be calculated for any specific concentration model. The concentration models of ENS01 and B01 are adopted in the calculations, while the DM profiles of subhalos used here are the NFW and Moore ones. The total number of subhalos $N(> 10^6 M_\odot)$ are calculated to be about 6400 in our Galaxy for NFW-ENS01, Moore-ENS01, NFW-B01 and Moore-B01 subhalo distributions.

In Fig. 6, we give the cumulative number of subhalos with $J_{\Delta\Omega(1^\circ)}$ larger than a specified value. From the figure we can see the number of subhalos with $J_{\Delta\Omega(1^\circ)} > 100$ depends on the concentration model and subhalo DM profile. Moore-B01 model provides the largest number of subhalos with high luminosity. There are several subhalos which are $J_{\Delta\Omega(1^\circ)} > 100$ in our galaxy in this model. For the Moore-ENS01 and NFW-B01 model, the subhalo number with $J_{\Delta\Omega(1^\circ)} > 100$ in 6400 subhalos is about 0.6 and 0.1 respectively and even smaller for the NFW-ENS01 model.

In order to show clearly the mass and location of subhalo with $J_{\Delta\Omega(1^\circ)} > 100$, we depict in Fig. 7 the number distribution in the $r - M_v$ map. Just for illustration purpose, the quantity inside the blue contour line shows the total number of these massive subhalos in the whole $M_v - r$ map. Outside the blue contour line, the number of such subhalos is zero. Moreover the quantity in the red contour line shows the subhalo number in the shadowed region. The figure shows that the subhalos tend to have moderate large mass. It is quite easy to understand. On one hand, subhalos with larger mass will induce higher $J_{\Delta\Omega}$. On the other hand, the number of higher mass subhalos is less. Thus the competition between these two effects determines that subhalos with moderate mass tend to provide the largest flux. The figure also indicates that subhalos tend to locate around 8.5 kpc from the GC, which is the distance between the GC and the Earth.

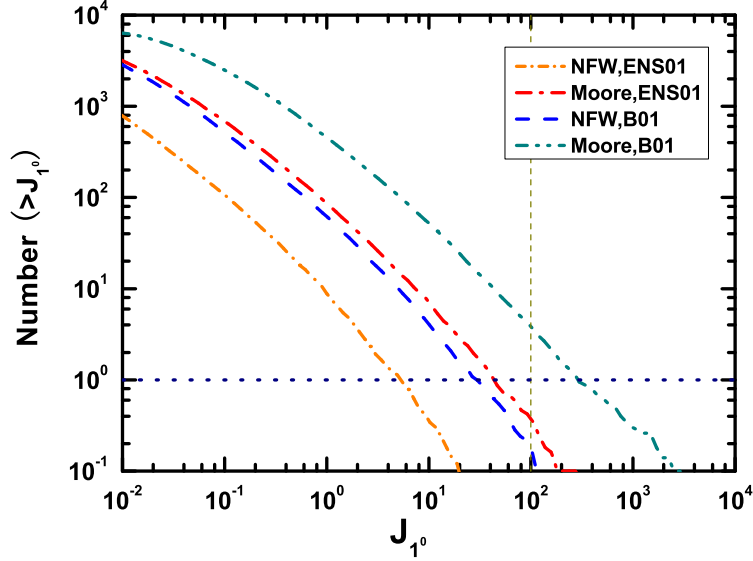


FIG. 6: The cumulative number of sub-halos with astrophysical factor $> J_{\Delta\Omega(1^\circ)}$ as a function of $J_{\Delta\Omega(1^\circ)}$. The dashed horizon line corresponds to the case that only one subhalo will be observed.

4. Summary

In this Appendix, we showed that the subhalos with $J_{\Delta\Omega(1^\circ)} > 100$ are very likely to have intermediate mass from $10^8 M_\odot$ to $10^{10} M_\odot$, and locate within several kpc from the Earth. The number of these subhalos in our Galaxy is about $O(1)$ which depends on concentration model and subhalo DM profile. It should be noted that the ENS01 and B01 models are for distinct halos in the Universe. In our Galaxy, the subhalos are in the host halo (Milky Way halo) which is denser than the Universe background. We can expect that the subhalos in the Milky Way halo should be more concentrated than the distinct halos. The simulation in Ref. [35] indeed shows the subhalos in a host halo have larger concentration parameter c_v than the distinct ones with the same mass. Thus we can expect larger number of high luminosity subhalos in our Galaxy comparing with the numbers above.

From Fig. 5 and Fig. 7, we can see that the whole subhalo may be difficult to be covered by the 1 degree half-cone, which means the subhalo can not be treated as ‘point source’. Nevertheless, we are interested in the bright core of subhalo which can still be processed as

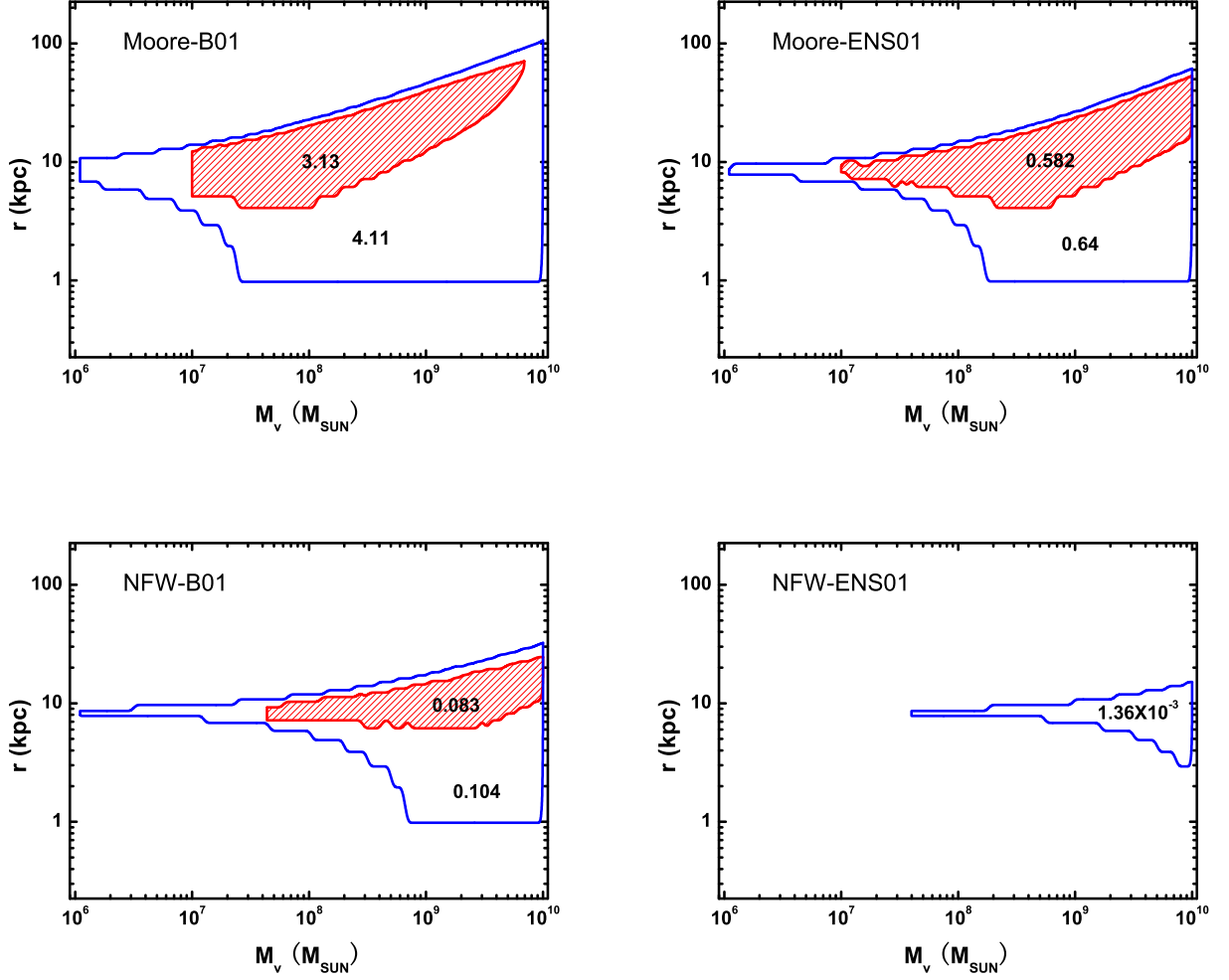


FIG. 7: The number distribution of subhalos with $J_{\Delta\Omega(1^\circ)} > 100$. The r is the distance from the GC, the M_v is the subhalo mass.

point source. The IceCube may discover these hot spots through survey of the sky map by 1 degree half-cone.

-
- [1] O. Adriani *et al.*, arXiv:0810.4995 [astro-ph]; arXiv:0810.4994 [astro-ph].
 - [2] J. Chang *et al.*, Nature **456**, 362 (2008).
 - [3] D. Hooper, P. Blasi and P. D. Serpico, arXiv:0810.1527 [astro-ph]; H. Yuksel, M. D. Kistler

- and T. Stanev, arXiv:0810.2784 [astro-ph].
- [4] L. Bergstrom, T. Bringmann and J. Edsjo, arXiv:0808.3725 [astro-ph]; V. Barger, W. Y. Keung, D. Marfatia and G. Shaughnessy, arXiv:0809.0162 [hep-ph]; I. Cholis, L. Goodenough, D. Hooper, M. Simet and N. Weiner, arXiv:0809.1683 [hep-ph]. M. Pospelov and A. Ritz, arXiv:0810.1502 [hep-ph]; M. Fairbairn and J. Zupan, arXiv:0810.4147 [hep-ph]. I. Cholis, D. P. Finkbeiner, L. Goodenough and N. Weiner, arXiv:0810.5344 [astro-ph]; Y. Nomura and J. Thaler, arXiv:0810.5397 [hep-ph]. D. Feldman, Z. Liu and P. Nath, arXiv:0810.5762 [hep-ph]; P. J. Fox and E. Poppitz, arXiv:0811.0399 [hep-ph].
- [5] M. Cirelli and A. Strumia, arXiv:0808.3867 [astro-ph]; M. Cirelli, M. Kadastik, M. Raidal and A. Strumia, arXiv:0809.2409 [hep-ph].
- [6] N. Arkani-Hamed, D. P. Finkbeiner, T. Slatyer and N. Weiner, arXiv:0810.0713 [hep-ph].
- [7] P. f. Yin, Q. Yuan, J. Liu, J. Zhang, X. j. Bi and S. h. Zhu, arXiv:0811.0176 [hep-ph]; K. Ishiwata, S. Matsumoto and T. Moroi, arXiv:0811.0250 [hep-ph]; C. R. Chen, F. Takahashi and T. T. Yanagida, arXiv:0811.0477 [hep-ph]; K. Hamaguchi, E. Nakamura, S. Shirai and T. T. Yanagida, arXiv:0811.0737 [hep-ph]; A. Ibarra and D. Tran, arXiv:0811.1555 [hep-ph]; C. R. Chen, F. Takahashi and T. T. Yanagida, arXiv:0811.3357 [astro-ph].
- [8] H. Baer, K. m. Cheung and J. F. Gunion, Phys. Rev. D **59**, 075002 (1999) [arXiv:hep-ph/9806361]; J. Hisano, S. Matsumoto, M. M. Nojiri and O. Saito, Phys. Rev. D **71**, 063528 (2005) [arXiv:hep-ph/0412403]; J. Hisano, S. Matsumoto, M. Nagai, O. Saito and M. Senami, Phys. Lett. B **646**, 34 (2007) [arXiv:hep-ph/0610249]. M. Cirelli, A. Strumia and M. Tamburini, Nucl. Phys. B **787**, 152 (2007) [arXiv:0706.4071 [hep-ph]]; J. March-Russell, S. M. West, D. Cumberbatch and D. Hooper, JHEP **0807**, 058 (2008) [arXiv:0801.3440 [hep-ph]]; J. D. March-Russell and S. M. West, arXiv:0812.0559 [astro-ph].
- [9] M. Lattanzi and J. I. Silk, arXiv:0812.0360 [astro-ph].
- [10] N. Itoh, H. Hayashi, A. Nishikawa and Y. Kohyama, ApJS 102: 411-424 (1996).
- [11] J. F. Beacom, N. F. Bell and G. D. Mack, Phys. Rev. Lett. **99**, 231301 (2007) [arXiv:astro-ph/0608090]; H. Yuksel, S. Horiuchi, J. F. Beacom and S. Ando, Phys. Rev. D **76**, 123506 (2007) [arXiv:0707.0196 [astro-ph]].
- [12] V. Barger, W. Y. Keung, G. Shaughnessy and A. Tregre, Phys. Rev. D **76**, 095008 (2007) [arXiv:0708.1325 [hep-ph]]; V. D. Barger, W. Y. Keung and G. Shaughnessy, Phys. Lett. B **664**, 190 (2008) [arXiv:0709.3301 [astro-ph]].

- [13] S. Palomares-Ruiz, Phys. Lett. B **665**, 50 (2008) [arXiv:0712.1937 [astro-ph]].
- [14] J. Liu, P. f. Yin and S. h. Zhu, Phys. Rev. D **77**, 115014 (2008) [arXiv:0803.2164 [hep-ph]].
- [15] P. f. Yin, J. Liu, Q. Yuan, X. j. Bi and S. h. Zhu, Phys. Rev. D **78**, 065027 (2008) [arXiv:0806.3689 [astro-ph]].
- [16] L. Covi, M. Greife, A. Ibarra and D. Tran, arXiv:0809.5030 [hep-ph].
- [17] S. Desai *et al.* [Super-Kamiokande Collaboration], Phys. Rev. D **70**, 083523 (2004) [Erratum-
ibid. D **70**, 109901 (2004)] [arXiv:hep-ex/0404025].
- [18] Y. Ashie *et al.* [Super-Kamiokande Collaboration], Phys. Rev. D **71**, 112005 (2005) [arXiv:hep-ex/0501064].
- [19] M. Ackermann *et al.* [The AMANDA Collaboration], Phys. Rev. D **71**, 077102 (2005) [arXiv:astro-ph/0412347]; M. Ackermann *et al.* [IceCube Collaboration], Astrophys. J. **675**, 1014 (2008) [arXiv:0711.3022 [astro-ph]].
- [20] M. D. Kistler and J. F. Beacom, Phys. Rev. D **74**, 063007 (2006) [arXiv:astro-ph/0607082];
J. F. Beacom and M. D. Kistler, Phys. Rev. D **75**, 083001 (2007) [arXiv:astro-ph/0701751].
- [21] E. Aslanides *et al.* [ANTARES Collaboration], arXiv:astro-ph/9907432.
- [22] J. Ahrens *et al.* [IceCube Collaboration], Astropart. Phys. **20**, 507 (2004) [arXiv:astro-ph/0305196].
- [23] J. Carr *et al.* [KM3NeT Collaboration], arXiv:0711.2145 [astro-ph].
- [24] J. F. Navarro, C. S. Frenk and S. D. M. White, Astrophys. J. **490**, 493 (1997) [arXiv:astro-ph/9611107].
- [25] P. Salucci, F. Walter and A. Borriello, arXiv:astro-ph/0206304.
- [26] M. Honda, T. Kajita, K. Kasahara, S. Midorikawa and T. Sanuki, Phys. Rev. D **75**, 043006 (2007) [arXiv:astro-ph/0611418].
- [27] T. Stolarczyk [ANTARES Collaboration], Nucl. Phys. Proc. Suppl. **165**, 188 (2007).
- [28] L. E. Strigari, S. M. Koushiappas, J. S. Bullock and M. Kaplinghat, Phys. Rev. D **75**, 083526 (2007) [arXiv:astro-ph/0611925].
- [29] R. Bruijn, PhD thesis, The Antares Neutrino Telescope: Performance studies and analysis of first data.
- [30] N. F. Bell and T. D. Jacques, arXiv:0811.0821 [astro-ph]; I. Cholis, G. Dobler, D. P. Finkbeiner, L. Goodenough and N. Weiner, arXiv:0811.3641 [astro-ph]; G. Bertone, M. Cirelli, A. Strumia and M. Taoso, arXiv:0811.3744 [astro-ph]; E. Nardi, F. Sannino and

- A. Strumia, arXiv:0811.4153 [hep-ph]; J. Zhang, X. J. Bi, J. Liu, S. M. Liu, P. f. Yin, Q. Yuan and S. H. Zhu, arXiv:0812.0522 [astro-ph].
- [31] A. Bhadra and R. K. Dey, arXiv:0812.1845 [astro-ph].
- [32] J. Hisano, M. Kawasaki, K. Kohri and K. Nakayama, arXiv:0812.0219 [hep-ph].
- [33] B. Moore, T. R. Quinn, F. Governato, J. Stadel and G. Lake, Mon. Not. Roy. Astron. Soc. **310**, 1147 (1999) [arXiv:astro-ph/9903164].
- [34] V. R. Eke, J. F. Navarro and M. Steinmetz, Astrophys. J. **554**, 114 (2001).
- [35] J. S. Bullock *et al.*, Mon. Not. Roy. Astron. Soc. **321**, 559 (2001).
- [36] J. Lavalle, Q. Yuan, D. Maurin and X. J. Bi, Astron. Astrophys. **479**, 427 (2008).
- [37] G. Tormen, A. Diaferio and D. Syer, Mon. Not. Roy. Astron. Soc. **299**, 728 (1998); A. A. Klypin, S. Gottlober and A. V. Kravtsov, Astrophys. J. **516**, 530 (1999). [arXiv:astro-ph/9708191]; B. Moore, S. Ghigna, F. Governato, G. Lake, T. Quinn, J. Stadel and P. Tozzi, Astrophys. J. **524** (1999) L19; S. Ghigna, B. Moore, F. Governato, G. Lake, T. Quinn and J. Stadel, Astrophys. J. **544**, 616 (2000). [arXiv:astro-ph/9910166]; V. Springel, S. D. M. White, G. Tormen and G. Kauffmann, Mon. Not. Roy. Astron. Soc. **328**, 726 (2001). [arXiv:astro-ph/0012055]; A. R. Zentner and J. S. Bullock, Astrophys. J. **598**, 49 (2003). [arXiv:astro-ph/0304292]; G. De Lucia *et al.*, Mon. Not. Roy. Astron. Soc. **348**, 333 (2004). [arXiv:astro-ph/0306205]; J. Diemand, B. Moore and J. Stadel, Nature **433**, 389 (2005) [arXiv:astro-ph/0501589].
- [38] J. Diemand, B. Moore and J. Stadel, Mon. Not. Roy. Astron. Soc. **352**, 535 (2004) [arXiv:astro-ph/0402160].
- [39] P. Madau, J. Diemand and M. Kuhlen, arXiv:0802.2265 [astro-ph].